arXiv:0807.2426v2 [cond-mat.stat-mech] 24 Oct 2008

# Finite temperature coherence of the ideal Bose gas in an optical lattice

Gevorg Muradyan and James R. Anglin
*Fachbereich Physik, TechnischeUniversität Kaiserslautern, D-67663 Kaiserslautern, Germany*

Abstract

In current experiments with cold quantum gases in periodic potentials, interference fringe contrast is typically the easiest signal in which to look for effects of non-trivial many-body dynamics. In order better to calibrate such measurements, we analyse the background effect of thermal decoherence as it occurs in the absence of dynamical interparticle interactions. We study the effect of optical lattice potentials, as experimentally applied, on the condensed fraction of a non-interacting Bose gas in local thermal equilibrium at finite temperatures. We show that the experimentally observed decrease of the condensate fraction in the presence of the lattice can be attributed, up to a threshold lattice height, purely to ideal gas thermodynamics; conversely we confirm that sharper decreases in first-order coherence observed in stronger lattices are indeed attributable to many-body physics. Our results also suggest that the fringe visibility 'kinks' observed in F.Gerbier et al., *Phys. Rev. Lett.* **95**, 050404 (2005) may be explained in terms of the competition between increasing lattice strength and increasing mean gas density, as the gaussian profile of the red-detuned lattice lasers also increases the effective strength of the harmonic trap.

## I. INTRODUCTION

The first investigations of dilute Bose-Einstein condensates (BECs) in periodic potentials [1, 2, 3] launched a research field which continues to expand steadily [4, 5]. The theoretical interest of the subject lies in the wide range of analogous phenomena for which it can provide an idealized model: spin-spin interactions in crystals [6, 7] and general Bose-Hubbard Hamiltonian dynamics[8], effective magnetic fields with non-abelian gauge potentials[9, 10], and even gravitational phenomena [11]. Experiments exploiting the high tunability of optical lattices have observed the Mott insulator phase transition [12, 13], the Berezinskii-Kosterlitz-Thouless transition[14], strong quantum depletion[15], extended coherency with number-squeezed states[16], second-order atom tunneling[17], resonantly enhanced tunneling[18], and repulsively bound atom pairs[19]. The combination of tunable optical lattices and ultracold temperatures provides enough control over atomic motion to investigate numerous questions of fundamental interest and importance.

A workhorse experimental technique for such investigations is the measurement of matter wave decoherence. Measurements of collective excitation spectra can provide independent information about many-body dynamics [12]; but such measurements are in general somewhat more involved. The coherent population fraction can be inferred fairly straightforwardly from measurements of fringe contrast in matter wave interference. A drop in coherent population fraction can signal the formation of interparticle correlations due to many-body interactions [20]. It can also be caused, however, by simple heating of the sample. Moreover, ramping up an optical lattice alters the density of states in a gas, and so can change its equilibrium properties even if heating as such can be suppressed. To use coherent population fraction as a signal of many-body physics, therefore, one must understand these background effects well enough to subtract them accurately.

The question of temperature and critical temperature change during the process of loading an optical lattice with atoms has already received substantial study [22, 23, 24, 25, 26, 27, 28, 29]. Unfortunately the problem turns out to be quite complicated in practice. While it is straightforward to show that ramping up a uniform lattice extremely slowly will adiabatically cool a non-interacting ultracold gas, interactions and a time-dependent trapping potential are unavoidable experimental complications. And although experiments are able to allow quite long times for the gas to equilibrate after the lattice has been fully turned on, the available experimental lifetimes set limits on how slowly the lattice potential can be ramped up, in order to reach full lattice strength before the gas escapes the trap. Under present conditions it therefore seems difficult to ensure that the gas really remains in equilibrium during the entire experiment. Some loss of condensate fraction does occur when the lattice strength is raised and lowered in a cycle, and although it is small enough to allow ample observations of Bose-Einstein condensates in optical lattices, it does indicate non-equilibrium entropy generation during ramping.

The theory of heating during loading of a condensate into an optical lattice is thus a subject of active research. It is an important task for cold atom theory, because direct experimental measurement of very low temperatures in highly condensed Bose gases remains technically difficult. (The standard fitting of the thermal fraction's momentum distribution to the Maxwell-Boltzmann formula becomes problematic when the thermal fraction is small.) The purpose of this paper is to study the effects of lattice potentials, as experimentally applied with focused laser beams and with harmonic trapping potentials superimposed, on the density of states of the ideal Bose gas. Our main contribution is to identify a basic competition between density of states and spatial density, which occurs because of the particular way optical lattices are implemented in current experiments, and which considerably moderates the effect of weaker lattices on gas coherence.

As a first exercise in identifying the quantitative consequences of these effects in experiments, we model several recent experiments under the simplifying assumptions that the gas does remain in global thermal equilibrium

at all times, and moreover that it maintains a constant temperature. We determine this temperature by fitting to experimental data from before the lattice potentials are ramped up. This scenario would be expected in the case where the trapped gas was maintained in equilibrium through scattering with a reservoir of thermal gas, which was itself too slightly perturbed by the time-dependent lattice to undergo any temperature change. For shallow lattices our isothermal model turns out to fit experimental data somewhat better than the alternative scenario of isentropic evolution optical lattices, which would be expected if the lattice-trapped gas could be regarded as isolated, and if the lattice were ramped up slowly enough for equilibrium still to be maintained. Our quantitative results thus provide some somewhat surprising input for the further non-equilibrium studies which will ultimately be required in this problem. Moreover, they serve to confirm the dynamical competition effect we identify, which must play an important role in determining how the gas coherence depends on the lattice potential, regardless of the precise statistical ensemble which should describe the gas.

The paper is organized as follows. We first indicate the parameter regime in which an ideal Bose gas in thermal equilibrium is expected to be a good model for experimental systems. We then describe the theory we will use for a Bose-condensed ideal gas in an optical lattice at finite temperature. Along with this full version of our ideal gas theory, whose predictions we will compute numerically, we introduce some further approximations that will allow analytical results, and help interpret our numerical curves.

We then present our numerical calculations and compare them with several sets of experimental data, including experimental configurations in which the gas dynamics is effectively three-, two-, or one-dimensional. In particular we consider the fringe visibility "kinks" seen in recent experiments, where the downward sloping curve of first order matter coherence versus increasing lattice strength has a shoulder. We show and explain a very similar effect in the ideal gas coherent fraction, which occurs at closely comparable lattice strengths.

In our final section we summarize our results and provide an outlook sketch.

## II. THERMAL EQUILIBRIUM

We assume interaction between particles sufficient to maintain equilibrium by Boltzmann scattering. In a truly collisionless regime, an adiabatic change of potential would simply preserve the population in each energy level, and so would not change the number of condensed atoms. In considering an ideal gas in equilibrium, however, we naturally mean that we consider time scales long enough for interactions in the form of collisions to generate the time-averaged behavior that is represented by a grand canonical ensemble; but we do not admit interactions strong enough to alter the instantaneous probability distributions in that ensemble, which therefore depends only on the non-interacting Bose gas Hamiltonian.

Cold dilute gases in experiments can certainly be made very weakly interacting, so the experimental relevance of our model depends on the relation between the experimental time scale $\tau_X$ and the timescale $\tau_C$ for collisional equilibration. Quantum kinetic theories for ultracold atoms support the identification of the latter timescale with Boltzmann's scattering time:

$$\tau_C = \frac{1}{8\pi a^2 \rho}\sqrt{\frac{m}{2k_B T}}, \tag{1}$$

where $\rho$ is the gas density, $T$ is the gas temperature, $a$ is the s-wave scattering length for low momentum transfer collisions, and $m$ is the particle mass. This gives an equilibration timescale on the order of $\tau_C \approx 40ms$ for $^{87}Rb$ with densities of $\rho \approx 10^{13} cm^{-3}$. Since lattice ramp time scales in experiments are generally much longer than this, our assumption of equilibrium because $\tau_C \ll \tau_X$ should be adequate for experimental comparison.

The validity of our ideal gas approximation then depends on the ratio between $\tau_C$ and the relevant time scale $\tau_D$ for single-particle dynamics. What then is this $\tau_D$? A global definition in terms of the rate of change of single particle energy eigenstates would be appropriate for experiments in the collisionless kinetic regime, studying the first onset of interaction effects. For current experiments approaching phenomena such as quantum phase transitions due to onsite interactions, a local criterion is more relevant. We therefore consider $\tau_D$ to be the time scale for quantum tunneling between two adjacent optical lattice sites. We can invoke the energy-time uncertainty relation to estimate this tunneling time as $\tau_D = \hbar/\delta E$ for $\delta E$ the width of the lowest energy band. At optical lattice depths of order $40E_r$ ($E_r = \hbar^2 k^2/2m$ being the 'recoil energy') this implies $\tau_D \approx 100ms$. For the strongest experimental lattices we thus have $\tau_D \gtrsim \tau_C$, so that particles typically collide before leaving one lattice site. The ideal gas approximation therefore breaks down, and interparticle interactions begin to have nontrivial effects beyond merely enforcing equilibrium over long time scales. Accurately assessing such effects is one of the major challenges in current many body theory; our goal in this paper is simply to identify the onset of this regime in current experiments.

For shallower optical lattices, however, the tunneling time rapidly decreases: $\tau_D \approx 1ms$ for a lattice depth of $12E_r$. With $\tau_D \ll \tau_C \ll \tau_X$, particles will typically tunnel through many lattice sites before scattering, so that the resulting equilibrium distribution of single-particle energies will include the band structure of the lattice, but the effects of harmonic trapping over length scales much longer than the lattice spacing can be computed in local density approximation. This theory should apply up to the onset of dynamically (as opposed to kinetically) significant interactions at high lattice potentials. As we will see, it does indeed fit experiments well up to threshold

lattice strengths. This agreement is not trivial, however, but depends upon the cancellation of two basic features of the single-particle dynamics in typical experimental potentials. The interaction onsets identified in this paper therefore provide useful information for interpreting experiments on ultracold atoms in optical lattices.

## III. MODEL POTENTIAL FOR OPTICAL LATTICE PLUS HARMONIC TRAP

We consider an ideal Bose gas in a harmonic trap to which has been added a periodic potential created by counterpropagating laser beam pairs in $x$, $y$ and $z$ directions. It turns out to be very important to represent the experimental fact that the focused red-detuned laser beams which generate the lattice potential have gaussian radial envelope profiles[30]:

$$V = \sum_{i=1}^{3} \left[ \frac{m\omega_{0,i}^2 r_i^2}{2} + V_i[\sin^2(kr_i) - 1]e^{\frac{-2(r^2-r_i^2)}{W_i^2}} \right] \quad (2)$$

Here $\omega_{0,i}$ is the angular frequency of the harmonic trapping potential in the $i$th direction, $k$ is the wavenumber of the 1D lattice potential formed by the AC Stark effect in the standing waves of the $i$th direction's laser pair, and $W_i$ is these beams' 'waist' (radius at which laser intensity has fallen by a factor $1/e^2$). We write $\sin^2(kr_i) - 1$ instead of $-\cos^2(kr_i)$ because we will treat differently the smooth gaussian envelope of the lattice minima and the gaussian modulation of the lattice barrier height.

The importance of the finite waist in the gaussian beam profile is as follows. All of these experiments use red-detuned light, so that the laser intensity maxima provide the lattice potential minima. This means that the AC Stark potential felt by the atoms is equivalent to a broad gaussian well, plus a repulsive lattice whose height diminishes with radius (according to the gaussian envelope). The spatial extent of the gas cloud is limited by the combined slowly-varying potential which is the superposition of the confining harmonic trap, plus the broad gaussian envelope of the attractive laser intensity maxima. Since the beam waist is in our cases much wider than the extent of the gas cloud in the trap, we can Taylor-expand the Gaussian profile of the beam, so that the envelope is approximately quadratic over the extent of the cloud. We must therefore consider that strengthening the lattice potential simultaneously strengthens the harmonic trapping confinement of the gas.

As well as the lattice potential minima becoming less deep towards the edges of the cloud, the height of the lattice barriers also decreases with radius; and this changes the local density of states for the atoms. For the experimental cases considered in this paper, however, the variation in the local width of the first energy band over the extent of the gas cloud is never greater than about 5%. This difference becomes even smaller for the stronger lattices that induce significant decoherence. We will therefore simplify our calculations considerably, at small cost in accuracy, by neglecting the effectively small local variation in lattice barrier height. The reason we can neglect the beam profile for the lattice barriers, but must include it in the attractive potential envelope, is that the relevant energy scale for the confining effect of the lattice minimum envelope is the gas chemical potential $\mu$, while the energy scale relevant to the effect of lattice height variation on bandwidth is at least $E_r$, which is much higher than $\mu$ in the cases we consider. We will therefore represent the potential induced by the red-detuned laser light as a superposition of a smooth harmonic well and a uniform repulsive lattice:

$$V \to \sum_i \left[ V_i \sin^2(kr_i) + \frac{m\omega_i^2 r_i^2}{2} \right] \quad (3)$$

where

$$\omega_i^2 = \omega_{0,i}^2 + \frac{4}{mW_j^2}V_j + \frac{4}{mW_l^2}V_l \quad (4)$$

for $i, j, l$ in cyclic order.

As a further technical simplification with negligible impact on the accuracy of our results, we will then replace the actual sinusoidal lattice with a parabolic spline potential, which is piecewise quadratic, and in particular is a periodic succession of upward and downward parabolas ('biparabolic'). As Fig.1 shows, this approximation is very accurate, but it will allow us to compute band structures more easily by taking advantage of analytical properties of confluent hypergeometric functions, instead of dealing with Mathieu functions. We will therefore finally write

$$V \to \sum_i \left[ V_i U(kr_i) + \frac{m\omega_i^2 r_i^2}{2} \right] , \quad (5)$$

having defined the periodic function

$$U(\xi) \equiv \frac{1-(-1)^n}{2} + (-1)^n \frac{2}{\pi^2}(\xi - n\pi)^2, \quad (6)$$

where the integer $n$ is chosen for given $\xi$ such that $(n - 1/2)\pi \leqslant \xi \leqslant (n + 1/2)\pi$.

For the uniform biparabolic lattice, (*i.e.* with $\omega_i$ set to zero in $V$ above), the single particle Schrödinger equation factorizes and the dispersion relation between energy and quasimomentum $\vec{p}$ is given by a some of one-dimensional energies,

$$E(\vec{p}) = \sum_{i=1}^{3} E_i(p_i) \ .$$

We show in the Appendix that the $E_i(p_i)$ can be found implicitly from dimensionless equations of the form

$$\cos\left(\frac{\pi p_i}{\hbar k}\right) = 1 - G\left(\frac{E_i}{E_r}, \frac{V_i}{E_r}\right) , \quad (7)$$

where $G$ is a particular combination of confluent hypergeometric functions [31] (see the Appendix). These equations can be solved numerically to produce an explicit numerical interpolating function for $E(\vec{p})$ in the uniform lattice, for any given lattice strengths $V_i$.

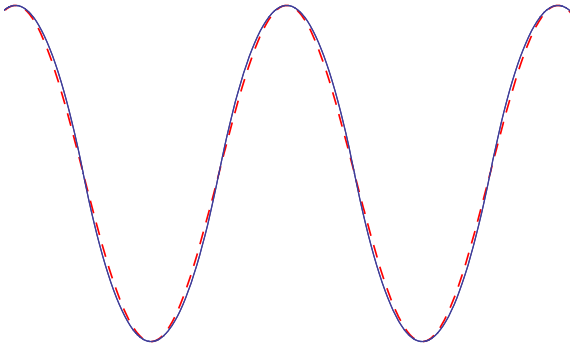


FIG. 1: Biparabolic periodic potential (solid line) used in this paper, in place of the actual sinusoidal lattice (dotted line).

## IV. THERMAL EQUILIBRIUM IN LOCAL DENSITY APPROXIMATION

We assume that the state of the (dynamically) non-interacting gas may be represented with a grand canonical ensemble, and this determines the number of non-condensed atoms $N_{NC}$ as a function of chemical potential $\mu$ and temperature $T$. We also take note of the fact that the gas density, locally averaged over a range of lattice cells, varies very slowly on the lattice scale. This allows us to use a local density approximation, as follows. We will consider

$$\tilde{\mu}(\vec{r}) \equiv \mu - \sum_{i=1}^{3} \frac{m\omega_i^2 r_i^2}{2} \tag{8}$$

for fixed $\vec{r}$ to be the 'local chemical potential', and compute the grand canonical density of non-condensed atoms $\rho(\vec{r})$ in the uniform lattice at temperature $T$ and chemical potential $\tilde{\mu}(\vec{r})$. We will then integrate over $\vec{r}$ to obtain the total $N_{NC}$. In the next Section we will then compare the theoretical $N_{NC}$ to the experimentally measured total particle number $N$, for various recent experiments. The difference $N_C = N - N_{NC}$ is inferred as the number of ideally Bose-condensed atoms. The coherency fraction $N_C/N$ will then be interpreted as the coherency fraction that would be expected in those experiments if only ideal gas physics were involved.

We therefore write

$$\rho(\vec{r}) = \frac{1}{(2\pi\hbar)^3} \int \frac{d^3p}{\exp\left[\beta(E(\vec{p}) - \tilde{\mu}(\vec{r}))\right] - 1}, \tag{9}$$

where $1/\beta \equiv k_B T$. We perform the $\vec{p}$ integrals using the so-called extended-zone scheme, integrating over quasi-momenta within the successive energy bands. In most cases we will be at low enough temperatures to restrict our integration to the first energy band only.

To now integrate over $\vec{r}$, we expand the Bose-Einstein denominator in a rapidly converging Taylor series to obtain

$$\begin{aligned} N_{NC} &= \int d^3r\, \rho \\ &= \sum_{n=1}^{\infty} \int \frac{d^3p}{(2\pi\hbar)^3} e^{-n\beta E(\vec{p})} \int d^3r\, e^{n\beta\tilde{\mu}(\vec{r})} \\ &= C \sum_{n=1}^{\infty} \frac{e^{n\beta\mu}}{n^{3/2}} \int d^3p\, e^{-n\beta E(\vec{p})} \end{aligned} \tag{10}$$

for

$$C \equiv \left(\frac{k_B T}{2\pi m\hbar^2}\right)^{\frac{3}{2}} \frac{1}{\omega_x\omega_y\omega_z}$$

and, since we are always considering samples in which some condensate is present,

$$\mu \to \sum_{i=1}^{3} E_i(0)\ .$$

We can perform the $\vec{p}$ integrals in the last line of Eqn. (10) numerically, for each $n$, using the $E(\vec{p})$ determined by numerically solving (7). The sum converges rapidly, and so we obtain a numerical figure for $N_{NC}$ for any given temperature $T < T_c$ and set of lattice strengths $V_i$. Eqn. (10), evaluated in this way, is the main result of this paper. In combination with experimental measurements of total particle number, and temperature estimates, it will provide the 'theoretical' curves plotted against experimental data in the next Section.

### A. Further approximations

Since our main result (10) is evaluated numerically, it is useful to compare it with simpler approximations whose physical content is more transparent. We will now present several of these, of which two will also be displayed, as dashed curves, in some of the next Section's plots.

As the periodic potential becomes stronger, the right-hand-side (RHS) of Eq.(7) approaches a linear function of $E_i/E_r$ (within each energy band). As an approximation that should become valid for high lattice barriers, therefore, we take the RHS to be an exactly linear function and obtain the following dispersion relation for the first energy band:

$$\begin{aligned} E_i(p_i) &= \frac{E_i^{\max} + E_i^{\min}}{2} - \frac{E_i^{\max} - E_i^{\min}}{2} \cos\left[\frac{\pi p_i}{\hbar k}\right] \\ &\equiv \bar{E}_i - \Delta_i \cos\left[\frac{\pi p_i}{\hbar k}\right]\ . \end{aligned} \tag{11}$$

Here $E^{\min}$ and $E^{\max}$ are the first energy band's boundary values. Although we determine these band edges from numerical calculations for our model lattice potential, this approximation for $E_i$ is of the same form obtained

in the well known tight binding approximation. We will therefore refer to this as the tight-binding approximation for $E(\vec{p})$. Using it, the $\vec{p}$ integral in (10) can be performed analytically over the first band, yielding

$$N_{NC}^{TB} \to (2\hbar k)^3 C \sum_{n=1}^{\infty} n^{-3/2} \prod_{i=1}^{3} e^{-n\beta\Delta_i} I_0\left(n\beta\Delta_i\right), \quad (12)$$

where $I_0$ is the modified Bessel function. Eqn. (12), referred to as 'the tight-binding approximation' for $N_{NC}$, will be used to generate the dashed curves in several Figures of the next Section.

For readers not intuitively familiar with modified Bessel functions, of course, this approximated expression is no more transparent than the more accurate numerical results of Eqn. (10). To indicate the dependence on the energy bandwidth more explicitly, however, we can simplify Eqn. (12) further in the strong lattice limit $\Delta_i \ll k_B T$, where the band*width* shrinks far below the temperature, but the temperature in turn remains well below the interband *gap*. In this limit we approximate the modified Bessel function as $I_0(0) = 1$ and obtain

$$N_{NC}^{TB} \approx Li_{3/2}\left(e^{-\beta\sum_{i=1}^{3}\Delta_i}\right) \prod_{i=1}^{3}\left[\frac{2}{\hbar\omega_i}\sqrt{\frac{k_B T E_r}{\pi}}\right], \quad (13)$$

where $Li_s(\xi) = \sum_{k=1}^{\infty} \xi^k/k^s$ is the polylogarithm function.

This simple formula shows well the qualitative impact of the lattice parameters on the noncondensed particle number. Strengthening the periodic potential compresses the energy bands, raising the density of states and thus increasing the noncondensed fraction. Increasing the harmonic trapping strength instead favors condensation, and hence tends to remove non-condensed atoms. Since the beam focus means that strengthening the lattice also strengthens the effective harmonic trap, these two effects compete as the lattice strength is ramped up.

This simple competition can also be seen, still using the tight-binding dispersion relation (11), but in the opposite temperture regime $\Delta_i >> k_B T$. Using the asymptotic form $I_0(\xi) \approx e^{\xi}/\sqrt{2\pi\xi}$ we obtain

$$N_{NC} = \zeta(3) \prod_{i=1}^{3}\left[\frac{k_B T}{\hbar\omega_i}\sqrt{\frac{2E_r}{\pi^2\Delta_i}}\right] \quad (14)$$
$$\equiv N_{NC}^{HO} \prod_{i=1}^{3}\sqrt{\frac{2E_r}{\pi^2\Delta_i}},$$

$N_{NC}^{HO}$ being the number of non-condensed bosons in a harmonic trap of frequencies $\omega_i$ at temperature $T$ [32]. ($\zeta(z)$ is the Riemann zeta function, and $\zeta(3) \doteq 1.202$). Neither of the two simplified formulas (13) and (14) will be compared with data in this paper, or for that matter referred to again at all; but they serve to illustrate qualitatively the competition between trap and band compression that is exhibited in the tight-binding approximation (15) and in the full theory of (10).

In the regime of temperatures much below the bandwidth, we expect most atoms to explore only the parabolic region of the dispersion relation, near its minimum. This immediately suggests, as an alternative to tight binding, the parabolic or effective mass approximation, in which the motion of particles in periodic structures is described as motion of free particle but with an effective mass (which is in general anisotropic):

$$\frac{1}{m_i^*} = \frac{\partial^2 E_i}{\partial p_i^2}\Big\rfloor_{\vec{p}=0}.$$

By Taylor expanding and keeping the first two terms on both sides of our dispersion relation Eq.(7), we obtain

$$m_i^* = \frac{2m}{\pi^2}\frac{\partial}{\partial\epsilon}G(\epsilon, V_i/E_r)\big\rfloor_{\epsilon=E_i(0)/E_r}.$$

Now approximating $E_i \to m_i^* p_i^2/2$ and integrating over the infinite range of $\vec{p}$, we find

$$N_{NC}^{EM} = \zeta(3) \prod_{i=1}^{3}\left[\frac{k_B T}{\hbar\omega_i}\sqrt{\frac{m_i^*}{m}}\right] \quad (15)$$
$$\equiv N_{NC}^{HO}\frac{\sqrt{m_x^* m_y^* m_z^*}}{m^{3/2}}.$$

Referred to as 'the effective mass approximation', this simplified formula will provide a second dashed curve for comparison in some of the Figures of the next Section.

Thus for low temperatures as well as for higher ones, and whether we assume tight binding or quasi-free motion, we see that the non-condensed particle number has on one hand a tendency to increase (at the expense of the condensate) as the lattice barrier height rises, because this raises the effective mass and compresses the energy bands. On the other hand the non-condensed number also tends to shrink, so that the condensate grows, when the harmonic confining potential is strengthened. And since experiments with focused red-detuned laser lattices make the barrier height and trapping potential rise and fall together, though not in direct proportion, a nontrivial competition is to be expected.

For temperatures within the bandwidth $\Delta_i$, the noncondensed particle number clearly depends on the details of the dispersion relation, and no simple approximation to Eqn. (10) will be very accurate. Our full numerical results for Eqn. (8), however, will still represent essentially this same competition between barrier height and containment.

Before comparing our results with several recent experiments, we pause to show that the competition between confinement and the barrier lattice is indeed important. The effectively increased harmonic confinement provided by a stronger red-detuned focused lattice can compensate to a considerable degree for the increased barrier height, and maintain a much higher condensate fraction than would survive if the total harmonic confinement were truly held constant. If we have a gas of $N = 1.5 * 10^5$ atoms in a harmonic trap with $\omega_{x,0}, \omega_{y,0}, \omega_{z,0} = 2\pi \times$

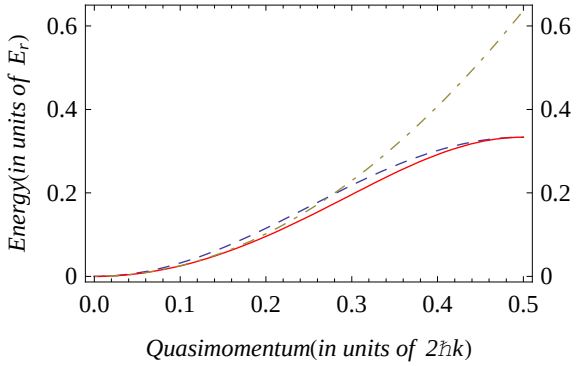



FIG. 2: First band energy-quasimomentum relation for the bi-parabolic lattice (solid line), in one dimension, with $V_i = 4E_r$. The dashed and dotdashed lines give the same dependance in the tight binding and effective mass approximations, respectively.

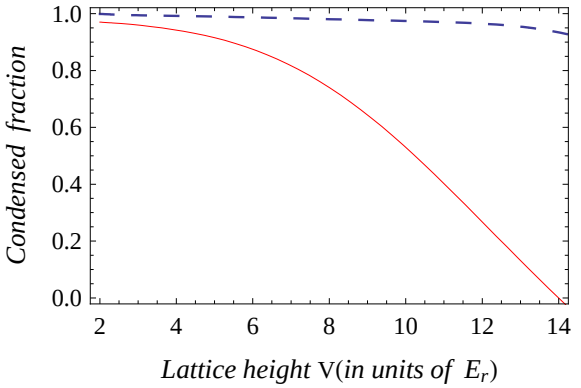



FIG. 3: Condensed fraction as a function of optical lattice height with (dashed) and without (solid) inclusion of the Gaussian profile of the beams.

$\{20, 20, 20\}$ $Hz$, and $T/T_C^0 = 0.3(15nK)$ is assumed to remain constant, then the condensate vanishes entirely at an optical lattice height of $14E_r$. Including the increased effective confinement, due to a gaussian beam profile with $1/e^2$ radii of 120 $\mu$m, changes the behavior completely: the condensate fraction $f_c = (N - N_{NC})/N$ changes by less than ten percent over this range of lattice heights. See Figure 3.

## V. COMPARISON WITH OBSERVATIONS

Figures. 4 through 7 show the results of our full numerical theory described above(isothermal) (Eq.(10)), plotted as a solid curve (red online), as well as of the two semi-analytic approximations (Eq.(12) for tight binding approximation and Eq.(15) for effective mass approximation) and of the isentropic evolution, when their inclusion is instructive. Superimposed for comparison are data points directly from the experimental publications. We take the experimentally measured total numbers $N$ of trapped particles, together with our theoretical values for non-condensed particle numbers $N_{NC}$, to compute the coherent fraction $f = 1 - N_{NC}/N$. The experimental values for coherent fraction were measured from interference fringe constrast.

We take all parameters directly from the published values for the experiments, with the exception of the gas temperatures. In the regime of very high condensate fraction, quantum gas thermometry is *experimentally* very difficult, and only a rough upper bound on the experimental temperature can be estimated ($T/T_C^0 \leq 0.36$, for example, in [13]). We have therefore taken temperature as a fitting parameter, tuning it so that our theoretical curve hits the first experimental data point (*i.e.* the one for lowest lattice strength). This may be considered an application of 'coherence thermometry': we use ideal gas thermodynamics in the lattice to infer the gas temperature from interference contrast measurements. We assume that the gas temperature remains constant, within the same experimental data set, for all other barrier heights. As already mentioned, this isothermal assumption is rather crude, and could certainly be improved upon by considering detailed quantum kinetic studies of the effects of changing lattice strength. The fact that interpretation of the data in line with our isothermal theory curves is nevertheless surprisingly straightforward is a significant point, therefore, even if it should turn out to be co-incidental, because it bears on the sensitivity of this type of experiment to quantum gas kinetics. We will discuss this issue further in our final section.

The various experiments we consider span the range of effective dimensionalities. In Fig.4 is shown the case where the lattice heights $V_i$ in all 3 directions are kept equal as they are ramped up, so that the gas is always effectively three-dimensional. The data for this case are taken from [13]. Our fitted temperature is $T = 45nK = 0.29T_C^0$, where $T_C^0$ is the critical temperature for BEC in the (rather elongated) experimental trap, which had $\{\omega_{x,0}, \omega_{y,0}, \omega_{z,0}\} = 2\pi \times \{20, 120, 120\}$ $Hz$.

In Fig. 4 we see that in the 3D geometry the noninteracting, isothermal gas's coherent fraction changes very little for lattice heights from $2E_r$ to $4E_r$. For stronger lattices than this, it monotonically decreases, until about $10E_r$; but at still higher lattice strengths, the coherence of the non-interacting gas actually increases slightly. This is because the stronger harmonic confinement of the gas is slightly over-compensating for the compression of the density of states in the stronger lattice. As one would expect, the tight-binding approximation approaches the full theory quite closely for strong lattices. The effective mass approximation becomes quite poor for stronger lattices, because it ignores the large band gap which is opening up. Since it includes thermal population of within-gap modes that do not actually exist, it greatly exaggerates the non-condensed population and hence underestimates the coherent fraction.

The theoretical curve for the isothermal ideal gas has

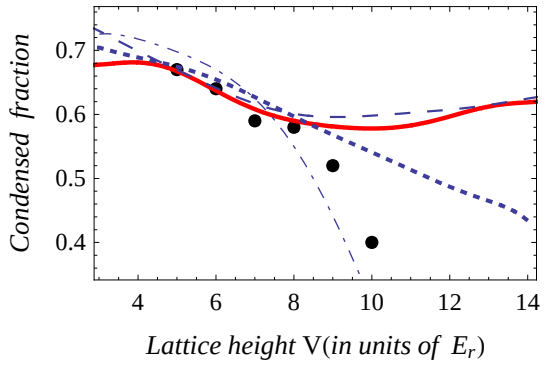



FIG. 4: Coherent fraction of ideal Bose gas (solid line) as a function of optical lattice height $V_i = V$, with all three lattice components equal in strength. The dashed and dot-dashed lines show the results under the tight-binding and parabolic approximations described in the text. The dotted line describes isentropic evolution. Points are experimental data taken from [13].

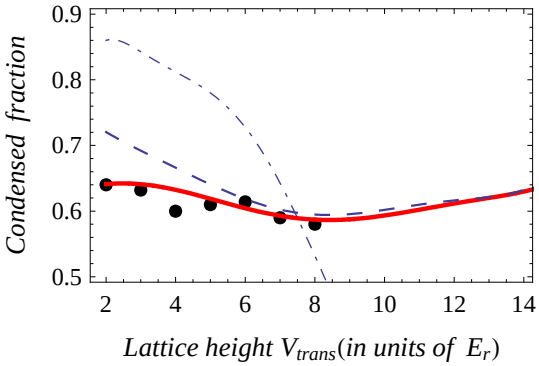



FIG. 5: Coherent fraction of the ideal Bose gas (solid line) as a function of transverse optical lattice height $V_{trans}$. The lattice strength along the long axis of the sample is held constant at $V_{ax} = 8E_r$. The dashed and dot-dashed lines give the same quantity under tight-binding and parabolic approximations, respectively. Points are experimental data taken from [32].

an excellent qualitative and quantitative agreement with experimental data for lattice heights up to $\sim 8E_r$, but thereafter the observed coherence of the real, interacting gas drops sharply. The fair agreement between the observations and the ideal gas in effective mass approximation is clearly co-incidental, since the drop in the effective mass approximation curve at this point is an error in its representation of the ideal gas. As the lattice becomes stronger, tunneling rates between lattice sites drop sharply, so that interactions become more and more important in comparison with kinetic energies, while the atomic interactions also become gradually greater as the gas becomes more tightly confined within each site. The ideal gas approximation gradually worsens, then breaks down abruptly at the Mott transition.

For this experimental case we have also computed the ideal gas coherent fraction assuming isentropic evolution, using a straightforward but computationally much more demanding version of our local density approximation. (Since entropy is an extensive variable, holding it constant is a non-local constraint.) As comparison between the solid and dotted curves of Fig. 4 shows, the distinction between isothermal and isentropic evolution is not dramatic for lattice strengths below those at which the ideal gas model itself breaks down. In detail, however, the isentropic dotted curve seems to do somewhat more poorly than the isothermal solid curve in fitting the 'shoulder' or 'kink' feature of the data, which although it is a small effect, is common to all currently available experiments. (This 'coherency saturation kink' will be discussed further below.) This fact would seem to be worth noting for future non-equilibrium studies of dilute Bose gases in time-dependent lattices.

In Fig.5 we compare our ideal gas theory with experimental data reported in [33]. In this case an effectively two dimensional situation was realized, by ramping up one component of the lattice to the rather high value of $8E_r$, and subsequently raising the lattice components in the other two orthogonal directions together, keeping them equal. Here our fitting happens again to find $T = 45nK = 0.29T_C^0$, while all the other parameters are as in [33]. Comparison shows that the ideal gas model still works very well for the same lattice height range of 2 to 8 $E_r$. The effective mass approximation is poor in this case because the lattice is always quite strong in one direction. A mixed approximation would presumably be better, assuming tight binding in one direction and a parabolic spectrum in the other two.

A quasi-one-dimensional version of this problem has also been realized [34], and is shown in Fig. 6. The trapped gas was in this case loaded into a strong two-dimensional lattice $40E_r$ high, and a weaker lattice potential along the axial direction $V_{ax}$ was raised to various much lower heights. In this case we see excellent agreement between the isothermal ideal gas theory and the experimental data, albeit in a regime where the variation is not dramatic in either one. To fit the initial experimental point, however, we have had to take a quite high temperature, nearly twice what the initial critical temperature would be in the same harmonic trap without the lattice: $T = 193nK = 1.94T_C^0$. (This harmonic trap had $\{\omega_{x,0}, \omega_{y,0}, \omega_{z,0}\} = 2\pi \times \{8.7, 90, 90\}\ Hz$.) With the strong transverse lattice and initial axial lattice at $V_{ax} = 2E_r$, however, the ideal gas critical temperature for BEC is actually $250nK$, so our fitted temperature was still well below the actual $T_c$. It is high enough, though, that the thermal occupation of the second axial band is non-negligible, and so in this case we have included it in

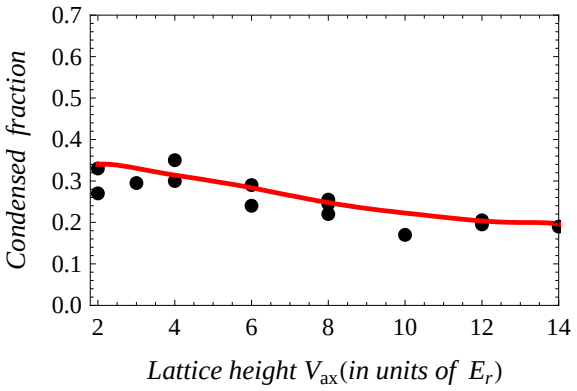



FIG. 6: Coherent fraction of the ideal Bose gas (solid line) as a function of axial optical lattice height $V_{ax}$. The lattice height in the other two directions is kept fixed at $V_{trans} = 40E_r$. Points are experimental data taken from [33].

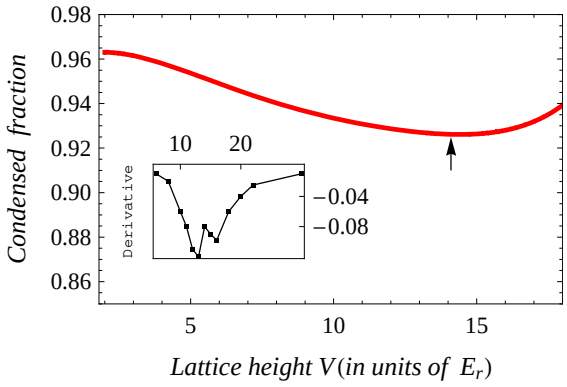



FIG. 7: Coherent fraction as a function of optical lattice height under experimental conditions of [34]. The arrow shows the point where the energy spectrum change due to harmonic trapping starts to dominate the change due to the periodic potential. The inset is data taken from [34], and gives a numerical derivative of the experimentally measured visibilty curve as a function of lattice height.

our full theory curve.

The temperature of the initial condensate in this experiment, before loading it into the lattice, was reported to be only around $50nK$. It is unclear, therefore, whether heating during this loading process has really raised the temperature by a factor of four, or whether many-body effects are already suppressing coherence at weak axial lattices because of the tight transverse confinement, or whether the high gas compression of the transverse lattice has simply raised the rate of scattering among atoms during the time-of-flight imaging process enough to degrade the observed interference patterns. The simplest explanation of Fig. 6, which is that turning on the strong transverse lattice had indeed considerably heated the samples, is by no means extremely implausible, however. The evidence from coherence for quantum many-body effects, as opposed to ideal gas thermodynamics, would seem to be weaker in the one-dimensional geometry than in the higher dimensionality cases.

### A. Coherency saturation

In all three cases discussed above, the initially falling theoretical curves level out, and then start to increase at some value of the potential height. This apparently counter-intuitive behavior of the non-interacting gas is in fact easily explained, as being due to the coincidental effective strengthening of harmonic confinement, along with strengthening of the lattice barriers, when the focused red-detuned laser intensities are raised. A stronger lattice means a narrower energy band, hence a greater density of states and larger non-condensed population, hence a lower coherent fraction. But a tighter trap at fixed (critical) chemical potential holds fewer non-condensed particles, and hence favors higher coherence. Which of these competing effects dominates depends upon the lattice and trap strengths and shapes. It also depends upon temperature. For temperatures ranging from $T = 30 - 60nK$ (which is $T \simeq 0.1 - 0.2T_C^0$ for the elongated trap of [35], with $\{\omega_{x,0}, \omega_{y,0}, \omega_{z,0}\} = 2\pi \times \{20, 200, 200\}\ Hz$), the lattice height at which the local coherency minimum occurs ranges over $V \sim 14 - 8E_r$. (Higher temperature brings the minimum to lower lattice heights.) Even for the ideal gas the quantitative details in this effect are involved, but the two competing factors are qualitatively simple and clear.

It seems worth bearing them in mind when investigating observations, as in [35], of 'kinks' in the coherence fraction curve for the real gases $\tilde{\text{N}}$ lattice heights at which the steady fall of coherent fraction seems to pause, before resuming. The fact that the coherency does resume falling, instead of rising as in the ideal case, is evidently due to interparticle interactions. And the true explanation of these coherency 'kink' observations may indeed have to do with the shifting of superfluid and Mott insulator shells with lattice height in the presence of the harmonic potential. But as Fig. 7 shows, when the number of atoms is $3.6 \times 10^5$ and the temperature is tuned to $T = 30nK$, the ideal gas coherency minimum is at $14E_r$, the same location seen experimentally. The fact that only mild re-tunings of the temperature are needed to make the ideal gas coherence curve show similar kinks at exactly the same lattice heights indicates that coherence enhancement because of rising effective harmonic confinement may also be playing a significant role at this point in the experimental system. It is beyond the scope of this paper, however, to assess the impact of this effect beyond the ideal gas regime.

## VI. CONCLUSION AND OUTLOOK

In this paper we have shown that optical lattices formed from red-detuned gaussian profile laser beams contribute an effective harmonic confinement to a trapped quantum gas, and that this effect needs to be taken into account in computing the coherence fraction of an ideal Bose gas in such a lattice at a given sub-critical temperature. It is in principle quite possible to remove this effect by altering the magnetic trap while raising the laser intensity, so as to hold the total harmonic confinement constant while the lattice is raised. We have shown that doing so would significantly simplify the interpretation of experimental results.

The good agreement between experiment and ideal gas theory that we have found up to threshold lattice heights supports the interpretation that many-body effects are slight up to that point, but that true many-body effects such as number squeezing and even the Mott transition do then appear, because ideal gas physics does not seem able to account naturally for the rather sharp drop in coherence observed at these points. It is important to note that the mildness of the variation with lattice height of the ideal gas's coherent fraction is largely due to cancellation between the lattice's band compression and the concomitant increase in harmonic trapping strength, as we have just summarized. Without this coincidental compensation through effective harmonic confinement, our Fig. 3 showed clearly that band compression at constant temperature can sharply lower the coherence of an ideal Bose gas in a strong optical lattice. It is therefore important to consider the effects discussed in this paper when inferring many body physics from coherency data.

A weak point in our theory as it stands is certainly the assumption that the temperature does not vary with lattice height. If the lattice is ramped on slowly enough for the cloud to remain in global equilibrium, and if the gas temperature is fixed by evaporation and heating processes that are insensitive to the lattice barrier height, then the isothermal assumption may well be valid. Determining precisely where observations depart from equilibrium ideal gas theory may also require more careful consideration, however. It seems quite plausible that our isothermal equilibrium curves are to some extent mimicking the more realistic combination of adiabatic cooling with non-equilibrium entropy generation. And perhaps, near the threshold lattice height, adiabatic cooling of the gas is able to compensate for some decoherence due to incipient number squeezing. If that were so, many body physics could actually be emerging somewhat before the experimental coherence fell below our isothermal theory curves. Or perhaps heating does increase before quantum many body effects really predominate, so that the first fall in coherence involves only ideal gas dynamics, and the onset of many-body dynamics comes only later. These issues will require further study, even just within ideal gas dynamics. Extension into weakly interacting dynamics, with mean field theory and Bogoliubov quasi-particles, is then an obviously desirable next step.

Finally, crude though its application in this paper has been, our temperature fitting procedure has raised the prospect of applying coherence thermometry in experiments on cold bosons in optical lattices, in regimes where normal time-of-flight thermometry becomes imprecise. Better theoretical calibration, taking into account the non-trivial kinetics issues described above, may make this a precise technique for future experiments.

## VII. APPENDIX

In this Appendix we derive the transcendental equation from which the dispersion relation in the uniform lattice may be determined numerically.

The one-dimensional time-independent Schrödinger equation for the biparabolic periodic potential may be written

$$\psi''(\xi) = (\lambda U(\xi) - \epsilon)\psi(\xi) \tag{A1}$$

where

$$\epsilon = \frac{E_i}{4E_r}$$
$$\lambda = \frac{V_i}{4E_r}$$
$$\xi = 2kx_i$$

and $U(\xi)$ is given by Eq. 6, which we re-write here:

$$U(\xi) \equiv \frac{1-(-1)^n}{2} + (-1)^n \frac{2}{\pi^2}(\xi - n\pi)^2 \ .$$

Linearly independent solutions of the equation A1 in the region $\pi/2 < \xi < 3\pi/2$ are

$$\varphi_1(\xi) = \exp\left(-\frac{\sqrt{\frac{2\lambda}{\pi^2}}(\xi-\pi)^2}{2}\right)\Phi\left(\alpha, \frac{1}{2}; \sqrt{\frac{2\lambda}{\pi^2}}(\xi-\pi)^2\right), \tag{A2}$$

$$\varphi_2(\xi) = (\xi-\pi)\exp\left(-\frac{\sqrt{\frac{2\lambda}{\pi^2}}(\xi-\pi)^2}{2}\right) \times \Phi\left(\alpha+\frac{1}{2}, \frac{3}{2}; \sqrt{\frac{2\lambda}{\pi^2}}(\xi-\pi)^2\right), \tag{A3}$$

where $\Phi(X)$ is a confluent hypergeometric function,

$$\alpha = \frac{1}{4}\left(1 - \frac{\epsilon}{\sqrt{\frac{2\lambda}{\pi^2}}}\right),$$

and thus the wavefunction in this region can be written as

$$\Psi_I = c_1\varphi_1(\xi) + c_2\varphi_2(\xi), \tag{A4}$$

whith unknown constant coefficients $c_1$ and $c_2$.

Correspondingly the linearly independent solutions in the "barrier-type" region $3\pi/2 < \xi < 5\pi/2$ are

$$\widetilde{\varphi}_1(\xi) = \exp\left(\frac{i\sqrt{\frac{2\lambda}{\pi^2}}(\xi-2\pi)^2}{2}\right) \times \Phi\left(\beta, \frac{1}{2}; -i\sqrt{\frac{2\lambda}{\pi^2}}(\xi-2\pi)^2\right), \tag{A5}$$

$$\widetilde{\varphi}_2(\xi) = (\xi-2\pi)^2 \exp\left(\frac{i\sqrt{\frac{2\lambda}{\pi^2}}(\xi-2\pi)^2}{2}\right) \times \Phi\left(\beta+\frac{1}{2}, \frac{3}{2}; -i\sqrt{\frac{2\lambda}{\pi^2}}(\xi-2\pi)^2\right), \tag{A6}$$

where

$$\beta = \frac{1}{4}\left(1 - i\frac{\epsilon-\lambda}{\sqrt{\frac{2\lambda}{\pi^2}}}\right),$$

and the wavefunction is

$$\Psi_{II} = \widetilde{c}_1\widetilde{\varphi}_1(\xi) + \widetilde{c}_2\widetilde{\varphi}_2(\xi), \tag{A7}$$

with unknown constant coefficients $\widetilde{c}_1$ and $\widetilde{c}_2$.

Using the Bloch theorem [36] we can write the wavefunction in the region $5\pi/2 < \xi < 7\pi/2$ as

$$\Psi_{III} = \exp\left[\frac{i\pi p}{\hbar k}\right]\Psi_I. \tag{A8}$$

Now implementing the continuity requirements of the wavefunctions and their derivatives at the boundary points $3\pi/2$ and $5\pi/2$, we get a homogeneous system for the unknown coefficients, and from the requirement of nontrivial solution we obtain the dispersion relation Eq.(7), with

$$G\left(\frac{E}{E_r}, \frac{V}{E_r}\right) = (\varphi_1(\xi)\widetilde{\varphi}_1'(\xi) + \widetilde{\varphi}_1(\xi)\varphi_1'(\xi)) \times (\varphi_2(\xi)\widetilde{\varphi}_2'(\xi) + \widetilde{\varphi}_2(\xi)\varphi_2'(\xi))\,|_{\xi=\pi/2}, \tag{A9}$$

with prime denoting the first order derivative.

This work was supported by the Alexander von Humboldt Foundation Georg Forster programme and The Marie Curie RTN EMALI (MRTN-CT-2006-035369).


[1] K. Berg-Sörensen and K. Mölmer, Phys. Rev. A **58**, 1480 (1998).
[2] D. Jaksch et al., Phys. Rev. Lett. **81**, 3108 (1998).
[3] B.P. Anderson, and M.A. Kasevich, Science **282**, 1686 (1998).
[4] O. Morsch and M. Oberthaler, Rev. Mod. Phys **78**, 179 (2006).
[5] I. Bloch et al., arXiv:0709.2094
[6] A. Sörensen and K. Mölmer, Phys. Rev. Lett **83**, 2274 (1999).
[7] L.-M. Duan, et al. Phys. Rev. Lett. **91**, 090402 (2003).
[8] D. Jaksch and P. Zoller, Annals of Physics **315**, 52 (2005).
[9] K.Osterloh et al., Phys Rev. Lett. **95**, 010403 (2005).
[10] J. Ruseckas et al., Phys Rev. Lett. **95**, 010404 (2005).
[11] S. Dimopoulous et al., Phys. Rev. Lett. **98**, 111102 (2007).
[12] M. Greiner et al., Nature **415**, 39 (2002).
[13] T. Stöferle et al., Phys. Rev. Lett. **92**, 130403 (2004).
[14] Z. Hadzibabic et al., Nature **441**, 1118 (2006).
[15] K.Xu et al., Phys. Rev. Lett. **96**, 180405 (2006).
[16] W. Li et al., Phys. Rev. Lett. **98,** 040402 (2007).
[17] S. Fölling et al., Nature **448**, 1029 (2007).
[18] C. Sias et al., Phys. Rev. Lett. **98**, 120403 (2007).
[19] K. Winkler et al., Nature **441**, 853 (2006).
[20] C. Orzel et al., Science **291**, 2386 (2001).
[21] A. Muradyan and A. Yalanuzyan, Opt. and Spec. **78**, 327 (1995).
[22] S. Burger et al., Europhys. Lett. **57**, 1 (2002).
[23] G. Muradyan and A. Muradyan, arXiv: cond-mat/0610797.
[24] P.B. Blakie and J.V. Porto, Phys Rev. A **69**, 013603 (2004); P.B. Blakie and A. Bezzet, Phys. Rev. A **71**, 013616 (2005); P.B. Blakie and Wen-Xin Wang, Phys. Rev. A **76**, 053620 (2007).
[25] K.P. Schmidt et al., Eur. Phys. J. D **38**, 343 (2006).
[26] A.M. Rey et al., Phys. Rev. A **73**, 023608 (2006).
[27] B. Capogrosso-Sansone et al., Phys. Rev. B **75**, 134302 (2007); B. Capogrosso-Sansone et al., Phys. Rev. A **75**, 013619 (2007).
[28] F. Gerbier, Phys. Rev. Lett. **99**, 120405 (2007).
[29] Tin-Lun Ho and Qi Zhou, Phys. Rev. Lett. **99**, 120404 (2007).
[30] R. Grimm et al., Adv. At. Mol. Opt. Phys. **42**, 95 (2000).
[31] A. Muradyan and G. Muradyan, arXiv: quant-ph/0204066.
[32] V. Bagnato et al., Phys. Rev. A **35**, 4354 (1987).
[33] C. Schori et al., Phys. Rev. Lett. **93**, 240402 (2004).
[34] L.Fallani et al., Phys. Rev. Lett. **98**, 130404 (2007).
[35] F. Gerbier et al., Phys. Rev. Lett. **95**, 050404 (2005); T. Greicke et al., J. Mod. Opt. **54**, 735 (2007).
[36] J.D. Patterson, B.C. Baily, *Solid State Physics, Introduction to Theory*, ( Springer-Verlag, Berlin 2007).